MIT Libraries | DSpace@MIT

MIT Open Access Articles

Optimal Design and Tolerancing of Compressor Blades Subject to Manufacturing Variability

Massachusetts Institute of Technology

Optimal Design and Tolerancing of Compressor Blades Subject to Manufacturing Variability

Eric Dow[*]and Qiqi Wang[†]

Massachusetts Institute of Technology, Cambridge, MA, 02139

This paper presents a computational approach for optimal robust design and tolerancing of turbomachinery compressor blades that are subject to geometric variability. This approach simultaneously determines the optimal blade geometry and manufacturing tolerances to minimize the overall cost of producing and operating the resulting compressor blades. A pathwise sensitivity method is used to compute gradient information that is in turn used to optimize the design and tolerances. Results for a two-dimensional subsonic compressor are presented, demonstrating the significant performance improvements that can be achieved using the proposed approach.

I. Introduction

The manufacturing processes used to create compressor blades introduce geometric variability, resulting in manufactured blades that deviate slightly from the design intent geometry. It has been observed that introducing geometric variability tends to negatively impact the performance of compressor blades. Not surprisingly, the variance of performance quantities of interest, such as the pressure ratio and adiabatic efficiency, are higher in the presence of manufacturing variability. Moreover, the mean pressure ratio and efficiency typically decrease in the presence of manufacturing variability.[1,2] This reduction in performance leads to increased operating costs over the life of the compressor blade, e.g. through increased fuel consumption.

The most direct means of improving performance is to impose stricter manufacturing tolerances, thereby reducing the level of geometric variability. However, this increases the cost of manufacturing. Although the resulting blades perform better, they are more expensive to produce. Alternatively, robust optimization techniques can be used to optimize the blade geometry to improve the probabilistic performance. It has been demonstrated that changing the level of geometric variability changes the optimal blade design resulting from a robust design optimization.[1] This suggests that the manufacturing tolerances should be designed alongside the compressor geometry. In this paper, we present a computational framework for simultaneously optimizing the blade design and tolerance scheme that takes both manufacturing cost and performance into account. This results in compressor blades that can be produced inexpensively and that perform robustly.

This paper consists of the following sections: section II describes a random field model of geometric variability and a related definition of manufacturing tolerances. Section III derives the non-linear optimization problem whose solution provides the optimal design and tolerance scheme. Section IV presents approaches for propagating variability and efficiently computing the sensitivity gradients used to solve the optimization problem. Results for a subsonic compressor are presented in section V, and conclusions and future work are outlined in section VI.

II. Modeling geometric variability and tolerances

Various approaches have been developed to model the geometric variations introduced by manufacturing processes. One approach is to construct probability distributions of geometric parameters such as camber, thickness, and chord using measurement data.[3–5] Principal component analysis (PCA) has also been used to

---

*PhD student, Department of Aeronautics and Astronautics, Room 37-442, MIT, Cambridge, MA 02139, AIAA Student Member

†Professor, Department of Aeronautics and Astronautics, Room 37-447, MIT, Cambridge, MA 02139, AIAA Member

characterize manufacturing variability.[1,6,7] PCA can be used to construct a probabilistic model of variability from the empirical mean and covariance of surface deviations at different locations on the blade.

In this work, we assume that the geometric variability in manufactured compressor blades can be accurately described as a non-stationary Gaussian random field $e(s, \omega)$ where $s \in \Omega_s$ parametrizes the location on the blade surface Ω_s. This model is similar to the PCA model developed by Garzon.[1] The primary difference in our approach is that the mean and covariance are provided in closed form, rather than being estimated from data. The random field $e(s, \omega)$ describes the error between the manufactured surface and the nominal surface in the normal direction at the point s on the nominal blade surface. This random field is defined by its mean $\bar{e}(s)$ and covariance function $C(s_1, s_2)$. The covariance captures the correlation between manufacturing errors at two different locations s_1 and s_2 along the blade surface, and describes the smoothness and correlation length of the random field.

The variance of the random field at the point s is equal to $C(s, s)$. The variance specifies the level of geometric variability, and is prescribed by the manufacturing tolerances. For stationary random fields, the variance is constant and $C(s, s) = \sigma^2$. The covariance function can then be written as $C(s_1, s_2) = \sigma^2 \rho(s_1, s_2)$ where $\rho(s_1, s_2)$ is the correlation function. In this work, the variance is specified as a spatially varying field $\sigma^2(s)$, which models the effect of spatially varying tolerances. In regions where the manufacturing tolerances are loose, the realized variability is large, and thus $\sigma^2(s)$ will also be large. Conversely, in regions where the tolerances are strict, $\sigma^2(s)$ is small. This is illustrated in figure 1, which depicts two different tolerance schemes near the leading edge of a compressor blade. The red regions around the black nominal geometry specify the tolerances, and the width of these tolerances vary around the blade.
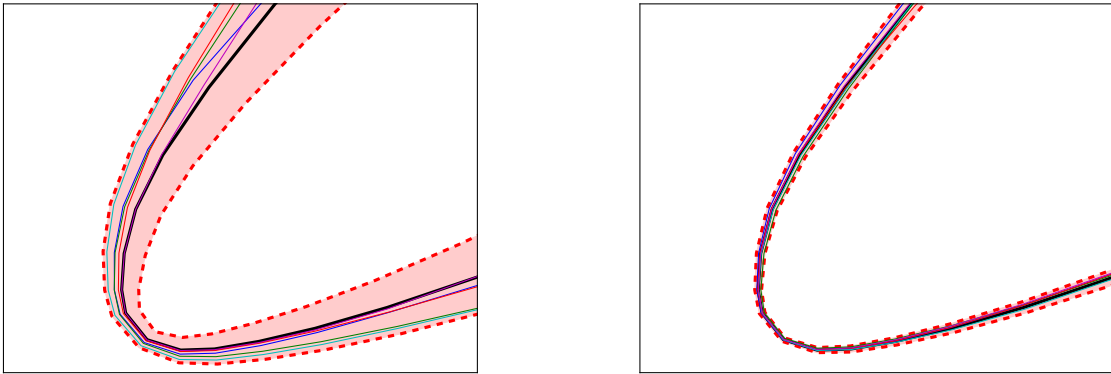

Figure 1. Depiction of loose (left) and strict (right) tolerances.

To achieve a non-stationary variance, the covariance function is written as

$$C(s_1, s_2) = \sigma(s_1)\sigma(s_2)\rho(s_1, s_2) \tag{1}$$

where $\rho(s_1, s_2)$ is assumed to be positive definite, i.e. $\rho(s_1, s_2) > 0$ for any s_1, s_2. It can be shown that the variance of the resulting random field is $\sigma^2(s)$.[8] We restrict $\sigma(s)$ to be positive everywhere, since it is practically impossible to achieve zero variance anywhere on the blade.

It was observed in the limited measurement data available that the geometric variations near the leading and trailing edges were more oscillatory than in other regions of the blade. This is likely the result of polishing processes used in the leading and trailing edges as part of the finishing process. To simulate this effect, a non-stationary correlation length model was used. Specifically, the correlation function was chosen to be

$$\rho(s_1, s_2) = \exp\left(-\frac{(s_1 - s_2)^2}{L^2}\right), \tag{2}$$

where the correlation length is given by $L = \sqrt{L'(s_1)L'(s_2)}$,

$$L'(s) = L_0 + (L_{LE} - L_0)\exp(-s^2/w^2). \tag{3}$$

American Institute of Aeronautics and Astronautics

The values $L_{LE} = 3.0 \times 10^{-3}$, $L_0 = 0.1$, and $w = 0.1$, all normalized by the blade half-arclength, were used.

To simulate realizations of the random field, we use the Karhunen-Loève expansion, which is constructed from the eigenvalues λ_i and eigenfunctions $\phi_i(s)$ of the covariance function:

$$e(s, \omega) = \bar{e}(s) + \sum_{i=1}^{\infty} \sqrt{\lambda_i} \phi_i(s) \xi_i(\omega) \tag{4}$$

The $\xi_i(\omega)$ are uncorrelated random variables with zero mean and unit variance.[9] For a Gaussian random field, the $\xi_i(\omega)$ are i.i.d. standard normal random variables. The eigenfunctions and eigenvalues are given by the Fredholm equation:

$$\int_{\Omega_s} C(s, s') \phi_i(s') ds' = \lambda_i \phi_i(s) \tag{5}$$

This integral equation is solved numerically on the discretized blade surface using the Nyström method with Gauss quadrature to approximate the integral.[10] The eigenvalues and discretized eigenfunctions are computed by solving a discrete eigenproblem. This results in a finite number of eigenvalues and eigenvectors, which is further truncated to give a stochastic dimension of N_{KL}. The truncation is determined by the decay of the eigenvalues.

III.   Simultaneous geometry and tolerance design

In the absence of geometric variability, the nominal blade geometry is determined by a vector of design variables $\boldsymbol{d} \in \mathbb{R}^{N_d}$, which are used by the design parametrization to produce the blade surface geometry. The performance of the compressor blade is characterized by a collection of engineering quantities of interest, e.g. the total pressure loss coefficient θ and total pressure ratio Π, which are computed from the flow field obtained by solving the compressible Navier-Stokes equations. The loss coefficient is computed as the difference between the mixed out total pressure and the theoretical isentropic exit total pressure divided by the inlet dynamic pressure:

$$\theta = \frac{p_{o2}^{\text{isen}} - \widetilde{p}_{o2}}{p_{o1} - p_1}. \tag{6}$$

Random geometric variations in the compressor blade surface result in random changes in the flow solution. The performance quantities derived from the flow solution thus become random variables. The loss coefficient, for example, can be described by a random variable $\theta(\omega)$ characterized by its probability density function. In general, changing the nominal blade design or the properties of the random manufacturing variations will change the distribution of the quantities of interest. The probabilistic performance of the compressor can be assessed by the moments of these distributions, such as the mean and variance.

As described previously, the tolerance scheme is specified through the variance field $\sigma^2(s)$. The standard deviation $\sigma(s)$ is discretized by introducing a basis $\{\psi_i(s)\}$:

$$\sigma(s) = \sum_{i=1}^{N_\sigma} \sigma_i \psi_i(s) \tag{7}$$

where σ_i are components of the tolerance design vector $\boldsymbol{\sigma} \in \mathbb{R}^{N_\sigma}$. We choose hat functions as our basis, since ensuring $\sigma(s) > 0$ is convenient for a nodal basis that is non-negative. For a given set of nodes on the blade surface, a hat function ψ_i is equal to one at s_i, and zero at all other nodes, decreasing linearly to the nodes neighboring s_i. Increasing one of the σ_i values has the effect of locally increasing the variance of the error field in the region of support of $\psi_i(s)$, which has the effect of loosening the tolerances in that region. Altering the properties of the manufacturing error field, i.e. its covariance function, results in a change to the flow solution and therefore to the moments of the quantities of interest. The connection between the performance moments and the nominal design and tolerances is illustrated in figure 2.

The relationship depicted in figure 2 suggests that is possible to optimize the probabilistic performance of the compressor blade by optimizing the nominal design variables and tolerance scheme simultaneously. The goal of this optimization is to obtain robust performance using compressor blades that are not overly expensive to produce. A combination of two cost functions, reflecting the probabilistic performance and
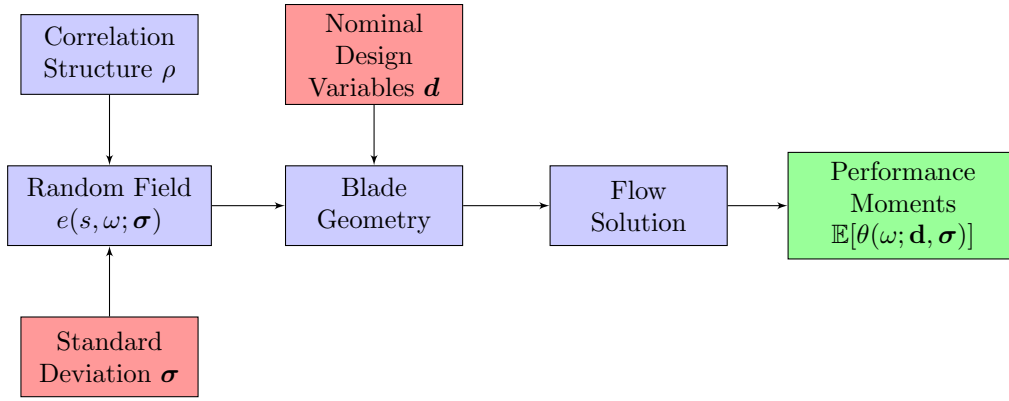
American Institute of Aeronautics and Astronautics

Figure 2. Relation between performance quantities of interest and the blade design and tolerance scheme.

manufacturing cost, are used to produce the desired design and tolerance schemes. The performance cost function is chosen to be the mean loss coefficient:

$$c_{\text{perf}}(\boldsymbol{d}, \boldsymbol{\sigma}) = k_m \mathbb{E}[\theta(\omega; \boldsymbol{d}, \boldsymbol{\sigma})] \tag{8}$$

where k_m is a constant. Reducing the loss coefficient reduces the specific fuel consumption. Thus, operating an engine with lower mean loss coefficient reduces the operation costs. The second cost function models the increase in cost resulting from reducing manufacturing tolerances:

$$c_{\text{man}}(\boldsymbol{\sigma}) = \int_{\Omega_s} \frac{1}{\sigma(s)} \, ds \tag{9}$$

Decreasing $\sigma(s)$, thereby allowing less geometric variability, increases the cost of producing each blade. This manufacturing cost model closely resembles those previously used in manufacturing tolerance optimization.[11]

To ensure adequate compression is achieved by the design, it is important to constrain the pressure ratio. The loss coefficient can be reduced by unloading the blade, and an optimizer will seek to exploit this effect, thereby reducing the pressure ratio. The mean total pressure ratio is therefore constrained to be greater than or equal to a threshold value $\bar{\Pi}_t$. Including this constraint into the optimization framework yields the following statement for the optimal blade design and tolerancing scheme $(\boldsymbol{d}^*, \boldsymbol{\sigma}^*)$:

$$
\begin{aligned}
\min_{\boldsymbol{d}, \boldsymbol{\sigma}} \quad & c_{\text{man}}(\boldsymbol{\sigma}) + c_{\text{perf}}(\boldsymbol{d}, \boldsymbol{\sigma}) \\
\text{s.t.} \quad & \mathbb{E}[\Pi(\omega)] \geq \bar{\Pi}_t \\
& \sigma_i > 0, \ i = 1, \dots, N_\sigma.
\end{aligned}
\tag{10}
$$

The total number of design variables $(N_d + N_\sigma)$ is in general large, motivating the use of gradient based optimization to solve (10). Methods such as sequential quadratic programming (SQP) are ideally suited to solving nonlinearly constrained optimization problems such as (10), and are used in this work.[12] In the next section, we discuss a computationally efficient approach for computing the gradients of the objective function and constraints.

IV.   Uncertainty propagation and sensitivity analysis

In order to solve the optimization problem (10), it is necessary to estimate the quantities $\mathbb{E}[\theta]$ and $\mathbb{E}[\Pi]$, as well as the sensitivities of these quantities to the design variables $\boldsymbol{d}$ and tolerance variables $\boldsymbol{\sigma}$. For simplicity, these moments are estimated using the Monte Carlo method, but more advanced quadrature schemes could also be used. The stochastic dimension, which is equal to the number of terms in the K-L expansion (4), is typically large. The Monte Carlo method is well suited to integration in high dimensions since its rate of convergence is independent of the stochastic dimension. The Monte Carlo estimate of the mean of the

American Institute of Aeronautics and Astronautics

loss coefficient, for example, is computed by sampling the random error field, and averaging the resulting functional value obtained for each sample:

$$\bar{\theta} = \frac{1}{N_{MC}} \sum_{n=1}^{N_{MC}} \theta_n, \tag{11}$$

where N_{MC} is the number of Monte Carlo samples used to estimate the mean. Other approaches to estimating the mean would result in similar summations over sample values of θ, with a different weighting appearing for each sample in the summation.

Although the convergence rate of the Monte Carlo estimate given by equation (11) does not scale with the stochastic dimension, it only scales as $N_{MC}^{-1/2}$. To reduce the variance in the Monte Carlo estimate and thus improve convergence, the antithetic variates method is used.[13] For each sample $\{\xi_1, ..., \xi_{N_{KL}}\}$, the corresponding antithetic sample $\{-\xi_1, ..., -\xi_{N_{KL}}\}$ is also taken. This is equivalent to choosing pairs of blade geometries with equal and opposite manufacturing errors. If the results obtained for the antithetic samples are negatively correlated, the variance of the Monte Carlo estimate is reduced. The magnitude of the manufacturing error is small, and the quantities of interest vary monotonically for small geometric perturbations. Thus, the antithetic variates method is able effectively to reduce the variance of the Monte Carlo estimates.

Since a gradient-based approach is used to solve (10), the gradients of the cost and constraint functions with respect to $\boldsymbol{d}$ and $\boldsymbol{\sigma}$ must be computed. In this work, the pathwise sensitivity method, which relies upon interchanging the differentiation and expectation operators, is used. For example, the sensitivity of the mean loss coefficient with respect to the nominal design variable d_j is computed as

$$\frac{\partial}{\partial d_j} \mathbb{E}[\theta(\omega)] = \mathbb{E}\left[\frac{\partial}{\partial d_j} \theta(\omega)\right] \tag{12}$$

which is unbiased if θ is smooth with respect to d.[14] The sensitivity $\partial\theta(\omega)/\partial d_j$ is interpreted as the sensitivity of the loss to the design variable d_j when the realization (or path) ω is fixed. In practice, this is achieved by fixing the random samples $\xi(\omega)$ in the K-L expansion in each step of the optimization. Replacing the expectation with its Monte Carlo estimate, we have

$$\frac{\partial\bar{\theta}}{\partial d_j} = \frac{1}{N_{MC}} \sum_{n=1}^{N_{MC}} \frac{\partial\theta_n}{\partial d_j}. \tag{13}$$

The sensitivity of the mean performance quantities with respect to the tolerance variables is computed in the same way:

$$\frac{\partial\bar{\theta}}{\partial\sigma_j} = \frac{1}{N_{MC}} \sum_{n=1}^{N_{MC}} \frac{\partial\theta_n}{\partial\sigma_j}. \tag{14}$$

The sensitivity $\partial\theta(\omega)/\partial\sigma_j$ represents the sensitivity of the loss with respect to changing to the variance for a fixed realization. By the chain rule, we have

$$\frac{\partial\theta_n}{\partial\sigma_j} = \frac{\partial\theta_n}{\partial e_n} \frac{\partial e_n}{\partial\sigma_j}. \tag{15}$$

The first term is a shape sensitivity, namely the sensitivity of the loss with respect to perturbing the error field. The second term is computed by applying the chain rule to the Karhunen-Loève expansion. When $\sigma(s)$ is perturbed, the eigenvalues λ_i and $\phi_i(s)$ of the K-L expansion are perturbed. Differentiating equation (4), we have:

$$\frac{\partial e_n}{\partial\sigma_j} = \sum_{i=1}^{N_{KL}} \left(\frac{1}{2\sqrt{\lambda_i}}\phi_i\frac{\partial\lambda_i}{\partial\sigma_j} + \sqrt{\lambda_i}\frac{\partial\phi_i}{\partial\sigma_j}\right)\xi_i(\omega). \tag{16}$$

The derivatives of the eigenvalues and eigenvectors are given by[15]

$$\frac{\partial\lambda_i}{\partial\sigma_j} = \phi_i^T \frac{\partial\mathbf{C}}{\partial\sigma_j}\phi_i, \tag{17}$$

American Institute of Aeronautics and Astronautics

$$\frac{\partial \phi_i}{\partial \sigma_j} = -(\mathbf{C} - \lambda_i I)^+ \frac{\partial \mathbf{C}}{\partial \sigma_j} \phi_i, \tag{18}$$

where $\mathbf{C}$ is the matrix resulting from the Nyström discretization of the Fredholm system (5) and $(\mathbf{C} - \lambda_i I)^+$ denotes the Moore-Penrose pseudoinverse of the matrix $(\mathbf{C} - \lambda_i I)$. Assuming that the eigenvalues $\{\lambda_i\}$ are unique, the pseudoinverse can be computed in a numerically stable manner since the dimension of the nullspace of $(\mathbf{C} - \lambda_i I)$ is one. Since the explicit dependence of the entries of the covariance matrix $\mathbf{C}$ on the σ_j is known via equation (1), the sensitivities of the eigenvalues and eigenvectors can be computed in closed form. The computational cost of computing the eigenvalue and eigenvector sensitivities is also negligible compared the computational cost of a typical flow solve.

The shape sensitivities $\partial \theta_n / \partial d_j$ and $\partial \theta_n / \partial e_n$ are computed using second order finite differences. For example,

$$\frac{\partial \theta_n}{\partial d_j} \approx \frac{\theta_n(d_j + \delta) - \theta_n(d_j - \delta)}{2\delta} \tag{19}$$

where δ is chosen sufficiently small. The computational cost of computing sensitivities is small since the perturbed flow solutions corresponding to $d_j + \delta$ and $d_j - \delta$ can be reconverged from the unperturbed flow solution with a few iterations.

V.   Results

To compute the flow solution and performance quantities of interest, the MISES (Multiple blade Interacting Streamtube Euler Solver) code is used.[16] MISES is a quasi-three-dimensional viscous flow solver, which solves the coupled Euler and integral boundary layer equations. The coupling of the inviscid and viscous regions is accomplished through the boundary layer displacement thickness. The non-linear system resulting from discretization of the coupled system is solved using Newton-Raphson iteration. Transition is modeled using a combination of the Abu-Ghannam-Shaw (AGS) bypass transition and e^n envelope models. The key advantage of MISES is its speed: a typical flow solution can be converged in a few seconds. Moreover, the required shape sensitivities can be efficiently computed with finite differences by reconverging the flow solution in a few iterations.

In this work, all geometries are strictly two-dimensional, resulting in a linear cascade of compressor blades. The blade surface is parameterized by the arclength s, starting at the trailing edge ($s = -1$), going around the leading edge ($s = 0$), and continuing back to the trailing on the opposite side of the blade ($s = 1$). All lengths are normalized by half of the arclength of the blade surface. MISES includes a blunt trailing edge model and the blade geometry is left "open" at the trailing edge. Thus, the impact of manufacturing variability at the trailing edge cannot be addressed using MISES. A modal perturbation approach was used to parameterize the nominal design geometry. Five Chebyshev modes were used, and the blade thickness was constrained by applying equal and opposite perturbations to corresponding points on the pressure and suction surfaces, reducing the effective number of modal design parameters to five. A rotational mode was added to control the blade stagger angle. The tolerances were parameterized with $N_\sigma = 31$ basis functions.

We consider a subsonic double-circular-arc (DCA) compressor blade developed by UTRC.[17] The mass flow rate is held constant by fixing the inlet Mach number to be $M_1 = 0.5$ and the inlet flow angle to be $\beta_1 = 41.9°$. Three separate optimizations are performed. The first is a deterministic optimization in the absence of geometric variability to minimize the loss coefficient (referred to as the "deterministic optimal" design hereafter). The pressure ratio is constrained to be greater than 1.158. The second is a robust optimization with a fixed level of variability ($\sigma = 5.0 \times 10^{-4}$, corresponding to a level of manufacturing variability similar to that found in high pressure compressor blades) is prescribed for the entire blade surface (referred to as the "robust optimal" design). This is equivalent to solving (10) with fixed $\sigma(s)$, so that only the nominal blade design is optimized. The final optimization is a simultaneous optimization of both the nominal design and manufacturing tolerances, with an initial manufacturing standard deviation of $\sigma = 5.0 \times 10^{-4}$ (referred to as the "tolerance optimal" design). For the robust and tolerance optimizations, $N_{MC} = 500$ Monte Carlo samples were used to estimate the mean loss and pressure ratio, as well as to compute the necessary gradients. The optimized nominal blade geometries are shown in figure 3. The optimized blades have reduced camber over the first half of blade, thereby shifting the loading of the blade further aft as illustrated by the plots of pressure coefficient shown in figure 5. The robust optimal and tolerance optimal geometries are quite similar. The optimal distribution of $\sigma(s)$ resulting from the simultaneous optimization

is shown in figure 4. The tolerances near the leading edge of the suction are reduced. Outside of this region, the tolerances are loosened significantly. Overall, the manufacturing cost function c_{man} is reduced by 49%.
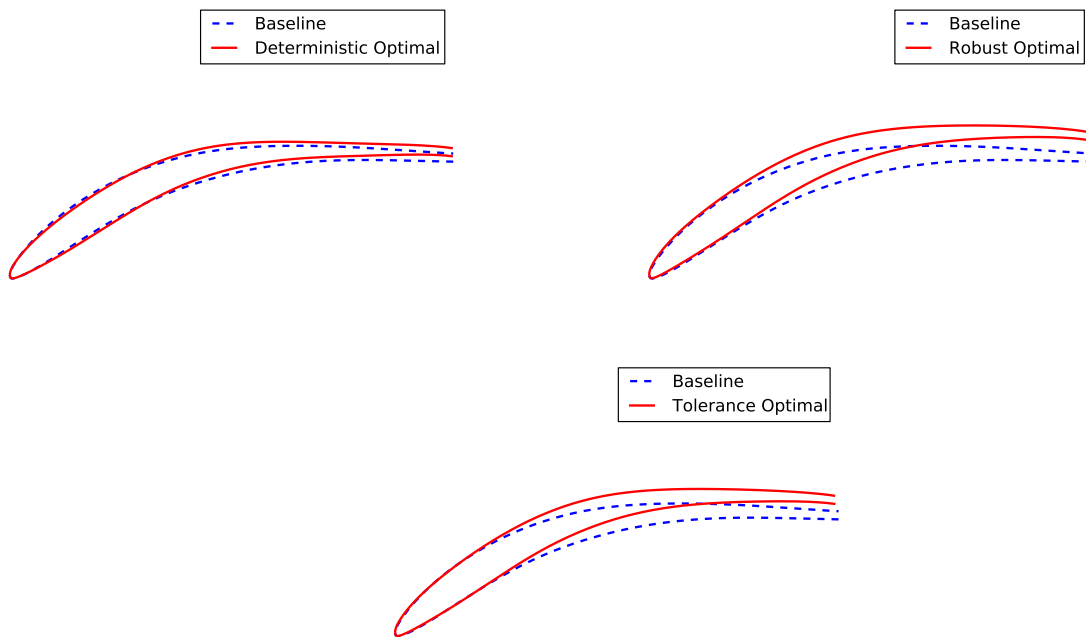

Figure 3. Optimal blade geometries (baseline UTRC geometry shown in dashed line).

Table 1 compares the relative performance of the various blade designs. For the baseline, deterministic optimal and robust optimal, the mean quantities are computed with $\sigma(s) = 5.0 \times 10^{-4}$. The optimized variance distribution depicted in figure 4 was used to compute the mean quantities for the tolerance design. In the absence of variability, the deterministic optimal design attains the minimum loss, as expected. When manufacturing variability is introduced, the performance of the baseline and deterministic optimal blades, as measured by the mean loss coefficient, degrades significantly. However, the mean loss coefficient for the robust and tolerance remains relatively unchanged in the presence of manufacturing variability. This illustrates the improved robustness of these two designs.

	Baseline	Deterministic	Robust	Tolerance
θ_0	1.721×10^{-2}	1.618×10^{-2}	1.632×10^{-2}	1.621×10^{-2}
$\mathbb{E}[\theta]$	1.753×10^{-2}	1.718×10^{-2}	1.644×10^{-2}	1.633×10^{-2}
$x_{tr,0}$	0.3078	0.3794	0.4198	0.4111
$\mathbb{E}[x_{tr}]$	0.2933	0.3253	0.4108	0.4049
Π_0	1.158	1.158	1.158	1.159
$\mathbb{E}[\Pi]$	1.158	1.158	1.158	1.159

Table 1. Nominal and mean performance values for the four blade geometries/tolerances.

Since the UTRC compressor is subsonic, the dominant loss mechanism is viscous loss generated in the boundary layer. The location of transition x_{tr} can have a large impact on the amount of loss generated
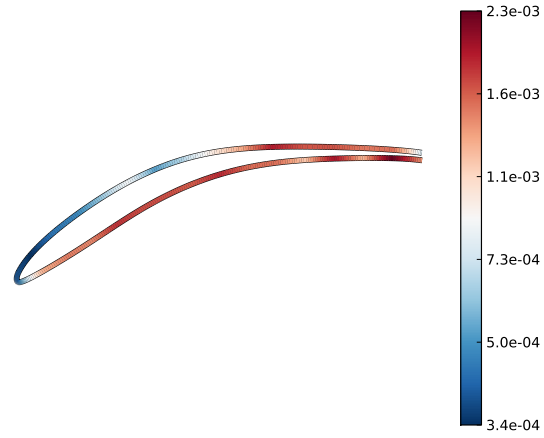
American Institute of Aeronautics and Astronautics

Figure 4. Optimized manufacturing tolerances.

(a) Baseline

(b) Deterministic Optimal

(c) Robust Optimal
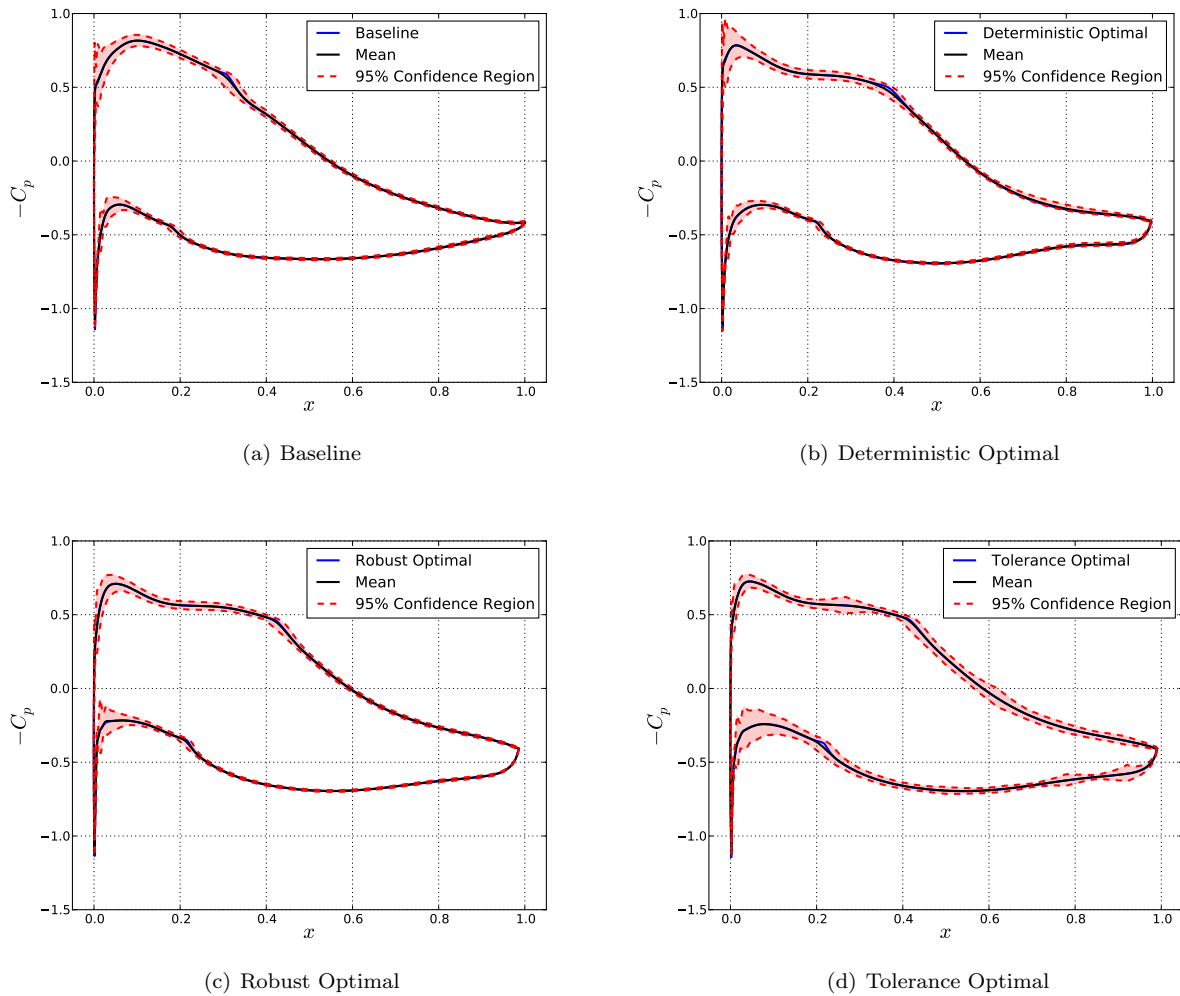

(d) Tolerance Optimal

Figure 5. Pressure coefficient distributions for the four blade geometries.

in the boundary layer, since the turbulent skin friction coefficient is higher than the laminar skin friction coefficient at a given Reynolds number. If the flow is not separated, as is the case for the UTRC compressor, delaying transition typically reduces the loss coefficient. Figure 6 illustrates the strong correlation between the suction side transition location and loss coefficient. The robust and tolerance optimal designs are able to delay transition for a significant fraction of sample geometries. This explains the increased robustness of these designs to manufacturing variations.
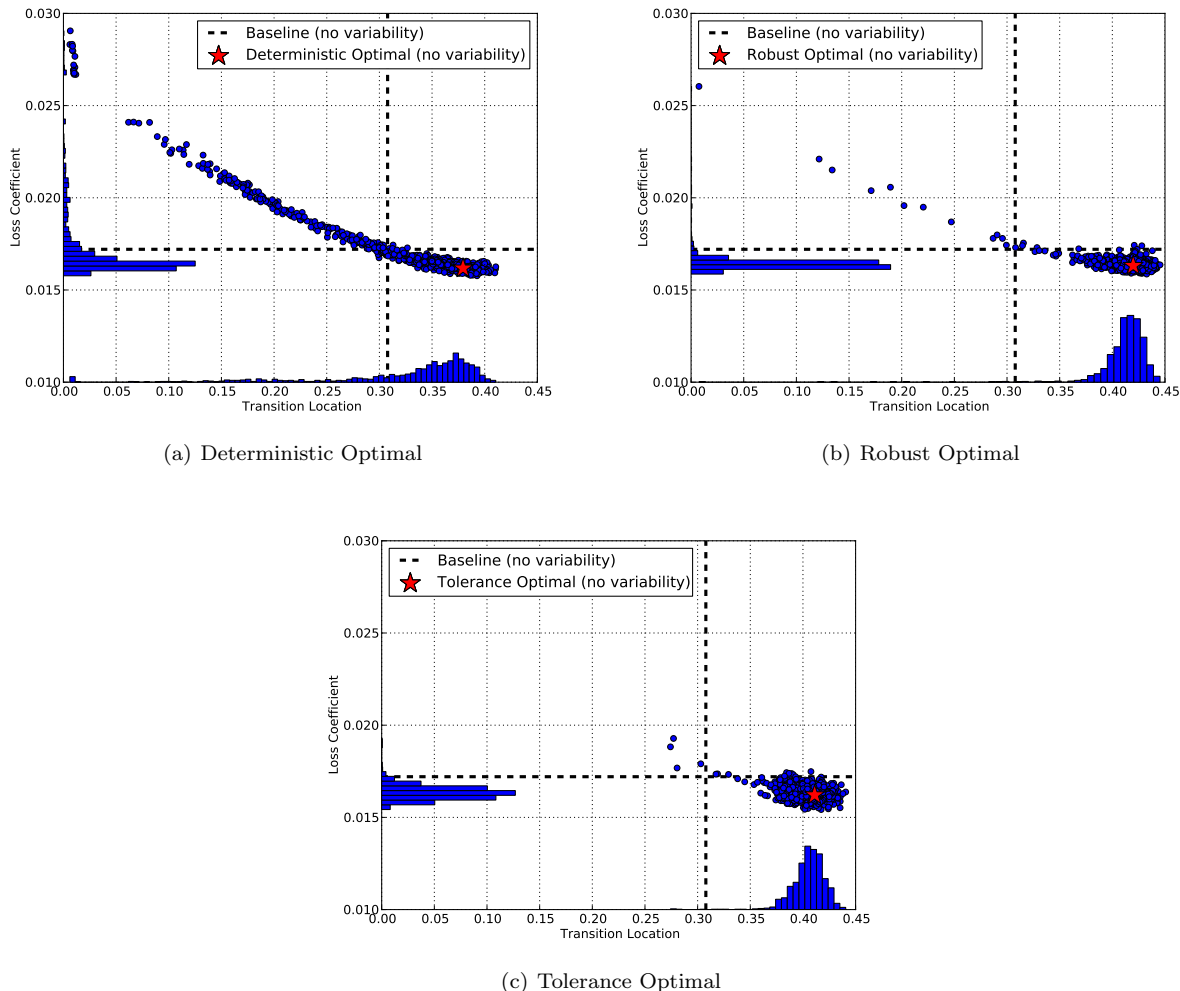

(a) Deterministic Optimal

(b) Robust Optimal

(c) Tolerance Optimal

Figure 6. Joint (dots) and marginal (bars) distributions of θ and x_{tr}.

To understand why the tolerance distribution shown in figure 4 is optimal, it is important to understand where the greatest losses are generated on the blade surface. Denton suggests using entropy creation as an effective measure of loss, and derives an expression for the viscous entropy generation rate (per unit span) up to the streamwise location s:[18]

$$\dot{S} = \int_0^s \frac{\rho_e U_e^3 C_{\mathcal{D}}}{T_e} ds, \tag{20}$$

where ρ_e, U_e and T_e are the density, velocity and temperature at the edge of the boundary layer, respectively. The dissipation rate is computed as

$$C_{\mathcal{D}} = \frac{1}{\rho_e U_e^3} \int_0^\delta \tau \frac{\partial u}{\partial y} dy. \tag{21}$$

Since the Mach number is low, the flow is nearly isothermal, and the differences in entropy generation between different geometries can be evaluated by comparing $\rho_e U_e^3 C_{\mathcal{D}}$. This quantity is plotted in figure 7 for the deterministic optimal design with no variability, as well as for the samples of the deterministic optimal

American Institute of Aeronautics and Astronautics

design subject to manufacturing variability with the smallest and largest values of x_{tr}, corresponding to the earliest and latest onset of transition. On the pressure side of the blade, the entropy generation past $s = 0.4$ is nearly identical for all three geometries. Since the total entropy generated on the pressure blade is the integral of $\rho_e U_e^3 C_\mathcal{D}$, it is not surprising that the difference between the generated entropy for the earliest and latest transition cases is very small. Clearly, the loss generated on the pressure side is insensitive to manufacturing variability, thus allowing for reduced tolerances on the pressure side, as illustrated in figure 4. The suction side of the blade is not as robust to geometric variation, as illustrated in the right plot. Early onset of transition increases the entropy production on most of suction side. Note also that the entropy production is roughly three times larger on the suction side than on the pressure side. The optimal tolerance scheme specifies low variability for a significant portion of the suction side to delay transition as much as possible.
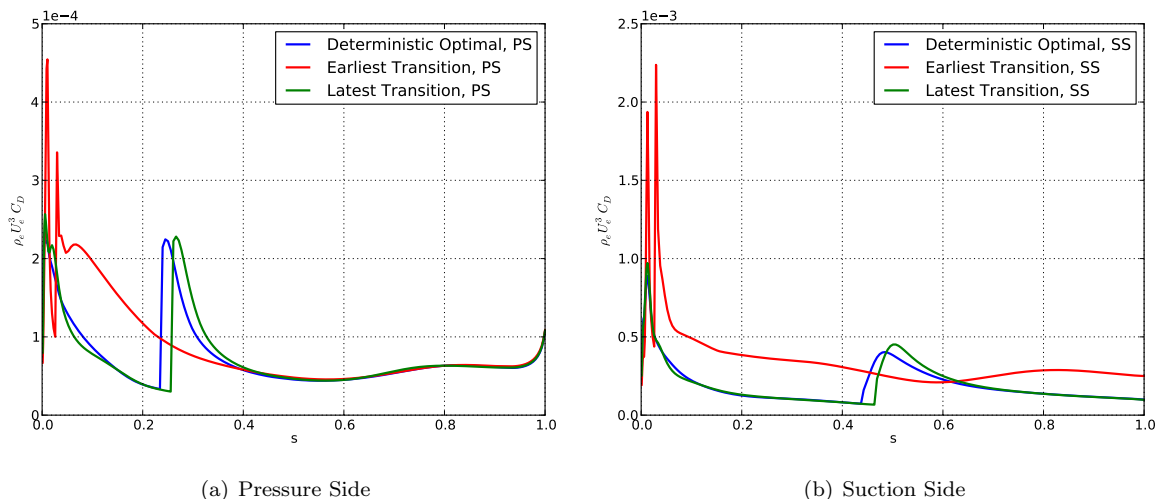

(a) Pressure Side (b) Suction Side

Figure 7. Comparison of $\rho_e U_e^3 C_\mathcal{D}$ on pressure and suction sides for the deterministic optimal design.

VI.   Conclusion and future work

A computational framework for performing simultaneous optimization of compressor blade design and manufacturing tolerances has been presented. This approach was successfully applied to optimize a blade geometry with increased robustness to manufacturing variability that can be produced at lower cost. For the subsonic cascade geometry considered in this paper, the optimal designs have reduced loading at the leading edge, and the optimal tolerance scheme reduces manufacturing tolerances near the leading edge. Analysis of the entropy production illustrates the importance of controlling geometric variability at the leading edge of the suction side of the blade.

Future work includes exploring more efficient methods for computing shape sensitivities, e.g. using the adjoint method, which can compute all shape sensitivities at roughly the cost of an additional flow solve. We also plan to explore the off-design performance of the optimized geometries, since only a single operating condition was considered in this work. Extensions to a transonic cascade, where shocks contribute to the loss, are also being pursued.

Acknowledgments

References

[1] Garzon, V. E., "Probabilistic Aerothermal Design of Compressor Airfoils," Ph.D. Dissertation, Department of Aeronautics and Astronautics, Massachusetts Institute of Technology, Cambridge, MA, 2003.

[2] Lange, A., Voigt M., Vogeler K., Schrapp, H., Johann, E., Gümmer, V., "Probabilistic CFD simulation of a high-pressure compressor stage taking manufacturing variability into account," ASME paper no. GT2010-22484, 2010.

[3] Lange, A., Vogeler K., Gümmer, V., Schrapp, H., and Clemen, C. "Introduction of a parameter based compressor blade model for considering measured geometry uncertainties in numerical simulation," *Proceedings of the ASME Turbo Expo 2009*, American Society of Mechanical Engineers, Orlando, FL, 2009.

[4] Heinze, K., Friedl, W.H., Vogeler, K., and Voigt, M., "Probabilistic HCF-Investigation of compressor blades," *Proceedings of ASME Turbo Expo 2009*, American Society of Mechanical Engineers, Orlando, FL, 2009.

[5] Javed, A., Pecnik, R., Olivero, M., and van Buijtenen, J.P., "Effects of manufacturing noise on microturbine centrifugal impeller performance," *Proceedings of ASME Turbo Expo 2012*, American Society of Mechanical Engineers, Copenhagen, Denmark, 2012.

[6] Häcker, J., "Statistical Analysis of Manufacturing Deviations and Classification Methods for Probabilistic Aerotheramal Design of Turbine Blades," Master's Dissertation, Derpartment of Aeronautics and Astronautics, University of Stuttgart, Stuttgart, Germany, 2000.

[7] Lange, A., Voigt, M., Vogeler, K., and Johann, E., "Principal component analysis of 3D scanned compressor blades for probabilistic CFD simulation," *Proceedings of the 53rd AIAA/ASME/ASCE/AHS/ASC Structures, Structural Dynamics and Materials Conference*, American Institute of Aeronautics and Astronautics, Honolulu, HI, 2012.

[8] Abrahamsen, P., "A review of Gaussian random fields and correlation functions, second edition," Norwegian Computing Center, TR-917, Oslo, Norway, 1997.

[9] Le Maître, O. P., and Knio, O. M., "Spectral Expansions," *Spectral Methods for Uncertainty Quantification*, 1st ed., Springer-Verlag, New York, 2010, pp. 17-44.

[10] Nyström, E. J., "Über die praktische Auflsung von Integralgleichungen mit Anwendungen auf Randwertaufgaben," *Acta Mathematica*, Vol. 54, 1930, pp. 185-204.

[11] Chase, K.W. and Greenwood, W.H., "Design Issues in Mechanical Tolerance Analysis," *Manufacturing Review*, Vol. 1, No. 1, 1988, pp. 50-59.

[12] Nocedal, J., and Wright, S. J., "Sequential Quadratic Programming." *Numerical Optimization*, 2nd ed., Springer-Verlag, New York, 2006, pp. 529-562.

[13] Hammersley, J.M. and Morton, W.K., "A new Monte Carlo technique: antithetic variates," *Mathematical Proceedings of the Cambridge Philosophical Society*, Vol. 52, No. 3, 1956, pp. 449-475.

[14] Glasserman, P., "Estimating Sensitivities," *Monte Carlo Methods in Financial Engineering*, Springer Verlag, New York, 2004, pp. 386-401.

[15] de Leeuw, J., "Derivatives of generalized eigen systems with applications," UCLA Department of Statistics, TR-528, Los Angeles, CA, Jan. 2007.

[16] Drela, M. and Youngren, H., "A User's Guide to MISES 2.63," MIT Aerospace Computational Design Laboratory, Cambridge, MA, 2008.

[17] Hobbs, D.E., Wagner, J.H., Dannenhoffer, J.F., and Dring, R.P., "Supercritical Airfoil Technology Program, Wake Experiments and Modeling for Fore and Aft-Loaded Compressor Cascades," Pratt & Whitney Aircraft Group, UTC, FR-13514, Hartford, CT, 1980.

[18] Denton, J.D., "Loss Mechanisms in Turbomachines," *Journal of Turbomachinery*, Vol. 115, No. 4, 1993, pp. 621-656.